Extremely large perpendicular magnetic anisotropy of an Fe(001) surface capped by 5*d* transition metal monolayers: A density functional study

D. Odkhuu,[1,*] S. H. Rhim,[1,3,†] N. Park,[2] and S. C. Hong[1,‡]

[1]*Department of Physics and Energy Harvest Storage Research Center, University of Ulsan, Ulsan 680-749, Korea*

[2]*Interdisciplinary School of Green Energy and Department of Physics, Ulsan National Institute of Science and Technology, Ulsan 689-798, Korea*

[3]*Department of Physics and Astronomy, Northwestern University, Evanston, IL 60208-3112, USA*

(Received 10 June 2013; revised manuscript received 9 September 2013; published 5 November 2013)

Significant enhancement of the magnetocrystalline anisotropy (MCA) of an Fe(001) surface capped by 4*d* and 5*d* transition metal monolayers is presented in this study using first principles density functional calculations. In particular, an extremely large perpendicular MCA of +10 meV/Ir was found in Ir-capped Fe(001), which originates not from the Fe but from the large spin-orbit coupling of the Ir atoms. From the spin-channel decomposition of the MCA matrix and electronic structure analyses, we find that strong 3*d*–5*d* band hybridization in the minority spin state is responsible for the sign changes of the MCA from parallel to perpendicular.

DOI: 10.1103/PhysRevB.88.184405 PACS number(s): 71.15.Mb, 75.70.Cn, 75.30.Gw, 75.50.Ss

I. INTRODUCTION

Magnetocrystalline anisotropy (MCA), the directional preference of magnetization, is a quantum phenomenon associated with magnetism and spin-orbit coupling (SOC) and is an issue of interest in spintronics. A prominent example is spin-transfer torque (STT) memory, which utilizes a spin-polarized tunneling current to switch magnetization.[1] In this application, a magnetic tunnel junction (MTJ) with perpendicular MCA (PMCA)—the preferential direction of the magnetization is normal to the film plane—provides significant advantages.[2,3] Recently, FeCoB films on MgO(001) capped by 4*d* or 5*d* transition metals (TMs) have drawn interest in the study of STT memory due to their large PMCA and high tunneling magnetoresistance.[3–5] However, the microscopic origin of the PMCA in these MTJs is unclear.[2] Ikeda *et al.*[3] and Wang *et al.*,[5] for instance, attributed the observed PMCA to contributions from the interface layer between the FeCoB and MgO. A few theoretical groups also addressed Fe/MgO and FeCo/MgO interfaces and have argued that the PMCA of the Fe(001) film is enhanced by the hybridization of Fe 3*d* orbitals with O p_z.[6,7] Nevertheless, recent experiments on TMs/FeCoB/MgO revealed evidence that the role of 5*d* or 4*d* orbitals is more decisive; in other words, that the 5*d* (4*d*) TMs/CoFeB interface is the origin of the observed PMCA.[8,9]

On the other hand, the magnetism in multilayers of 4*d* and 5*d* TMs grown on body-centered cubic (bcc) Fe substrate has been a long-standing subject of both experiment[10–15] and theory.[16,17] The 4*d* and 5*d* TMs (Ru, Rh, and Pd[10–13] and Os, Ir, and Pt[14,15]) isovalent to Fe, Co, and Ni exhibit ferromagnetic (FM) ground states at certain thicknesses. Numerous *ab initio* studies have shown that 4*d* and 5*d* atoms can possess induced magnetism in particular conditions,[16–22] which can be classified into two categories: (i) spontaneous magnetism from a structural change such as reduced dimension,[18,19] volume expansion,[20,21] or crystal structures that differ from naturally existing ones;[22] or (ii) induced magnetism from strong hybridization with magnetic metals.[16,17]

The 4*d* and 5*d* magnetism can lead to a larger MCA than conventional 3*d* magnetism because of stronger SOC. For instance, in a Co atom, a large MCA of 9.3 meV/atom (about 200 times larger than that in bulk Co) was observed in Co adsorbates on a Pt substrate.[23] Theoretical studies predict that extremely low-dimensional 4*d* and 5*d* TM systems, such as atomic dimers[24,25] and atomic chains,[18,19] can have fairly large MCAs on the order of tens of meV/atom, which are enhanced even more as the interatomic distances increase. Moreover, the small MCAs of Co and Fe are enhanced when Co monolayers (ML) on Au(111)[26] and Fe MLs on Pt(001) surfaces[27] are capped by additional Au and Pt layers, respectively.

In this paper, the MCAs of 4*d* and 5*d* TM MLs on bcc Fe(001) substrate [TM/Fe(001)] were investigated using the first principles full-potential linearized augmented plane-wave (FLAPW) method. We found that the presence of 5*d* TM MLs gave rise to an unexpectedly large PMCA due to their large SOC of 5*d* orbitals and hybridization with Fe 3*d*. Detailed analyses of the spin-channel and the atom-by-atom decompositions of the MCA of 5*d* TM/Fe(001) in comparison to the free-standing 5*d* TM MLs provide physical insights into the origin of the PMCA. These findings suggest a reasonable explanation for experimentally observed PMCAs of MTJs. The TM/magnetic interface plays a key role in determining the PMCA of the MTJs, even though the role of an insulator/magnetic interface cannot be ruled out by this study.

II. COMPUTATIONAL DETAILS

FLAPW[28] was employed for all calculations using both the generalized gradient approximation (GGA)[29] and the local density approximation (LDA)[30] for the exchange-correlation functional. Muffin-tin radii of 2.2 a.u. for Fe and 2.4 a.u. for 4*d* and 5*d* TMs were used. Cutoffs of 12.25 Ry and 256 Ry were chosen for the plane-wave basis and the charge density/potential representation, respectively. For integration in the Brillouin zone (BZ), 300 *k*-points were sampled in the irreducible wedge of a two-dimensional (2D) BZ. The convergence of total energy with respect to plane-wave cutoff and number of *k*-points was checked, and a strict self-consistent density criteria of 1×10^{-5} e/(a.u.)^3 was imposed.

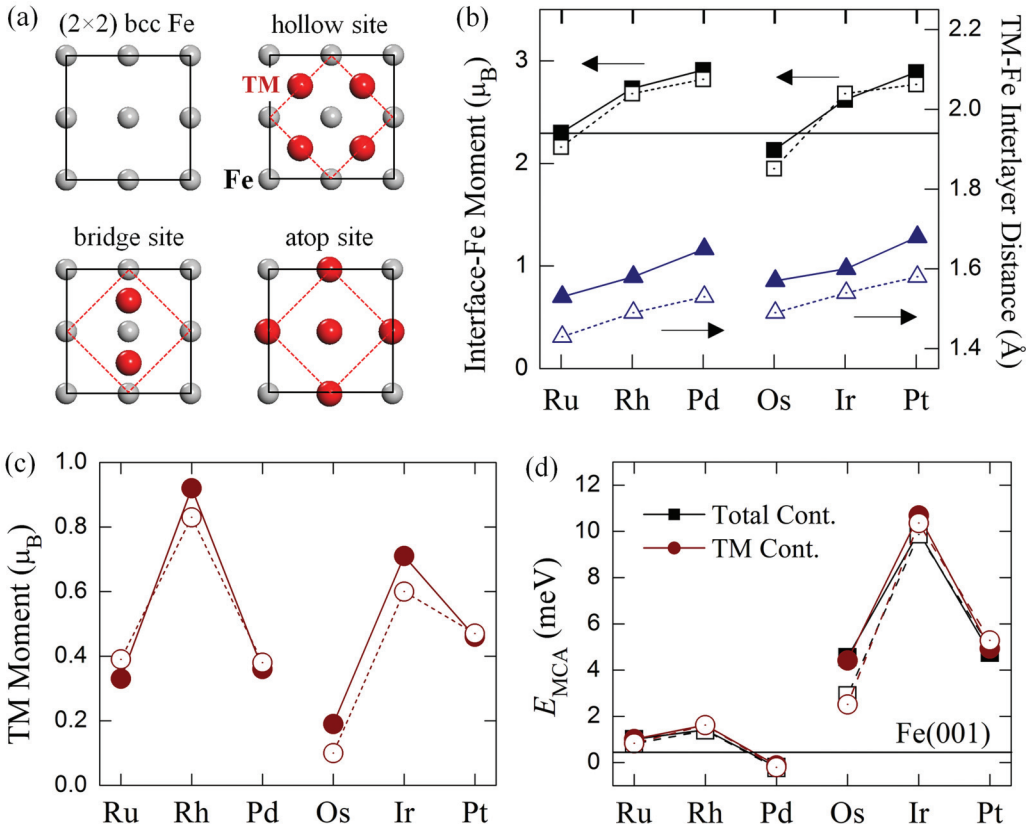

FIG. 1. (Color online) (a) Top view of (2 × 2) unit cell of TM/Fe(001) for hollow, bridge, and atop adsorption sites of TM atoms: gray balls represent Fe, and red represents TM atoms. The in-plane lattices of (2 × 2) bcc and (1 × 1) fcc lattices are shown by solid and dashed lines, respectively. (b) Magnetic moments (squares) of the interface Fe and interlayer distances (triangles) between the TM overlayer and the interface Fe. The horizontal line indicates the magnetic moment of the center Fe layer. (c) Induced spin moments of 4*d* and 5*d* TM atoms in TM/Fe(001). (d) Total E_{MCA} (squares) in meV/cell and contributions from 4*d* or 5*d* TM overlayers (circles) in meV/atom. The horizontal solid line represents the total E_{MCA} [meV/(surface atom)] of the clean Fe(001) surface. The results in GGA (LDA) are denoted by solid (open) symbols in all panels.

We modeled the system as a single slab consisting of five atomic layers of Fe and a ML of TM with *z*-reflection symmetry (each layer contained one atom). The single slab has true film geometry without introduction of artificial periodicity along the *z* direction, which is a unique feature of the FLAPW method.[28] The in-plane lattice constant of 2.87 Å was taken from the experimental lattice constant of bcc Fe. In the lateral cell, a ($\sqrt{2} \times \sqrt{2}$) lattice of bcc Fe was adapted to the (1 × 1) lattice of face-centered cubic TMs with lattice mismatches of 3.5% (Pt)–6.5% (Rh), as depicted in Fig. 1(a). Regarding the TM/Fe interface, we considered three TM adsorption sites: hollow, bridge, and atop site, with the hollow site being the most energetically favorable by 0.5–1.5 eV/cell. The TM and Fe atoms were fully optimized by atomic force calculations. To determine MCA energies (E_{MCA}), we used the torque method,[31] which has well-established validity and reliability.[32]

III. RESULTS AND DISCUSSION

The interlayer distances between TM ML and the interface Fe layer and the magnetic moments of the interface Fe atoms of 4*d* and 5*d* TMs/Fe(001) are shown in Fig. 1(b). The GGA (LDA) results are denoted by solid (open) symbols throughout this paper. The choice of exchange-correlation functional, either GGA or LDA, affect the interlayer distances by about 0.1 Å but not the magnetic moments of the interface Fe. As the atomic number increases in the 4*d* and 5*d* TMs from the Fe group to the Ni group, the interlayer distances increase monotonically, which agrees well with experiments: 1.43 Å for Ru (Ref. 13) to 1.63 Å for Pt (Ref. 15). The calculated magnetic moments of the interface Fe exhibit a trend similar to the interlayer distances. The Fe surface atoms capped by the Ni-group elements, Pd and Pt, have a large magnetic moment of about 3 μ_B per atom. The interlayer distances and magnetic moments of the Fe layers below the interface Fe are confirmed to be similar to those in the Fe center layer, indicating that the interface effect of the 4*d* and 5*d* TM overlayers was confined to the interface Fe atoms, as reported in a previous theoretical study.[33]

Induced spin moments of the TMs and the E_{MCA} values for TM/Fe(001) are presented in Figs. 1(c) and 1(d), respectively. The Co-group elements, Rh and Ir overlayers, are found to have the largest moments: 0.92 (0.83) and 0.71 (0.60) μ_B in GGA (LDA). This agrees with experimental[10–15] and theoretical studies.[16,17] All of the TM/Fe(001), except Pd/Fe(001), have positive E_{MCA} values, indicating that the direction of magnetization perpendicular to the film plane (PMCA) is energetically favored over the in-plane direction. Notably, the perpendicular

TABLE I. Energy difference between FM and NM states, $\Delta E = E_{FM} - E_{NM}$, magnetic moment (M), and E_{MCA} of the free-standing 5*d* MLs with the in-plane lattice constant (2.87 Å) of body-centered cubic (bcc) Fe.

Monolayers	ΔE (eV/atom)	M (μ_B/atom)	E_{MCA} (meV/atom)
Osmium	−0.11	1.44	+22.0
Iridium	−0.11	1.53	−5.78
Platinum	−0.03	0.65	−4.22

E_{MCA} of 5*d* TM/Fe(001) are significantly larger than those of 3*d* TM/Fe(001) (not shown) and 4*d* TM/Fe(001). In particular, the Ir-capped Fe(001) film exhibits the largest $E_{MCA} = +10$ meV/(surface atom), which is larger than that [+0.45 meV/(surface atom)] of the clean Fe(001) surface by more than an order of magnitude. We attribute the substantial enhancement of E_{MCA} in 5*d* TM/Fe(001) to the strong SOC of the 5*d* orbitals because the SOC is proportional to the fourth power of the atomic number. Note that within the 4*d* and 5*d* TM series, the magnetic moment of TM and E_{MCA} both exhibit a similar Λ-shaped trend; Rh and Ir have the largest magnetic moments and E_{MCA} values. This fact is closely related to hybridization and the band-filling effect, as will be discussed later.

The contribution to E_{MCA} from the individual atom was analyzed using the atom-by-atom decomposition of E_{MCA} for TM/Fe(001). The total and TM contributions to E_{MCA} are shown in Fig. 1(d). Note that the TM atoms contribute dominantly to E_{MCA}, whereas those from the Fe atoms contribute less than 5%, mostly from the interface Fe. For simplicity, our discussion will be focused on the enhanced E_{MCA} of 5*d* TM/Fe(001) rather than 4*d* TM/Fe(001).

To further clarify the role of the TM, the magnetism of the free-standing TM MLs was investigated using the same in-plane lattice constant as TM/Fe(001). Here, we show only the GGA results since the LDA results did not differ quantitatively. Table I shows the total energy differences between the FM and nonmagnetic (NM) states, $\Delta E = E_{FM} - E_{NM}$, magnetic moments, and E_{MCA} of the free-standing 5*d* TM MLs. In all 5*d* TM MLs, the FM states are energetically favorable, in agreement with previous work.[18,19,24,25] In these low dimensional systems, band narrowing enhances the densities of states (DOSs) at the Fermi level (E_F), thereby satisfying the Stoner criteria.

A comparison between Fig. 1(c) and Table I indicates that the presence of the Fe substrate reduces the spin magnetic moments of the 5*d* TM MLs substantially; Os has the most prominent reduction, leading to the Λ-shaped pattern in Fig. 1(c). Furthermore, the E_{MCA} of 5*d* TM/Fe(001) [Fig. 1(d)] show features markedly different from those of the free-standing 5*d* TM MLs (Table I). The E_{MCA} of the Os ML (about +22 meV/Os) is reduced to one-fifth of its magnitude when it is positioned on Fe(001). The negative E_{MCA} of the free-standing Ir and Pt MLs (−5.78 meV/Ir and −4.22 meV/Pt) become positive, about +10 meV/Ir and +4.9 meV/Pt, in the presence of the Fe(001) substrate. This implies that the Fe(001) substrate or the interface significantly influences the direction of the magnetization of the TM overlayers. This is a result of the hybridization between the Fe 3*d* and TM 5*d* orbitals, of which evidence will be shown later.

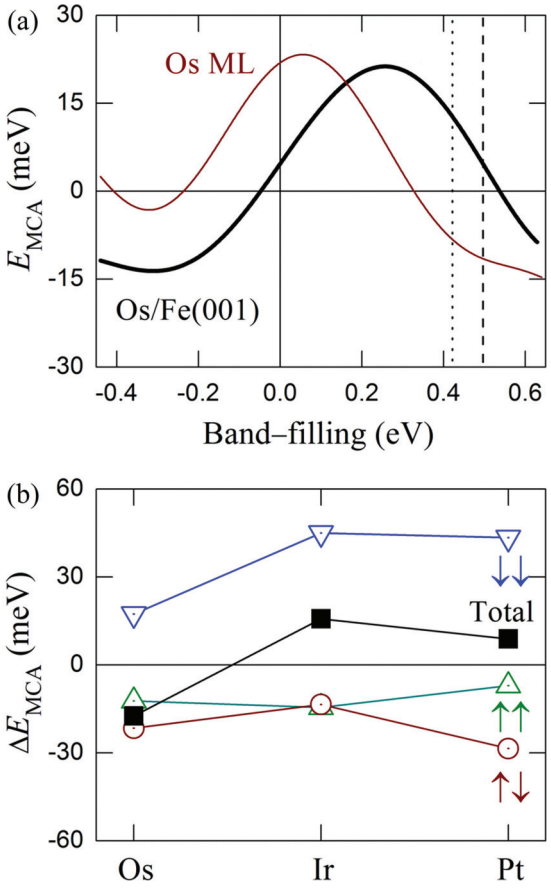

FIG. 2. (Color online) (a) The band-filling dependence of E_{MCA} on the free-standing Os ML (thin line) and Os/Fe(001) (thick line). Zero band filling is set to the Fermi level. The vertical dotted and dashed lines correspond to the estimated Fermi levels of Ir and Pt, respectively. (b) E_{MCA} difference (ΔE_{MCA}) between 5*d* TM/Fe(001) and 5*d* TM ML for the spin-channel contributions of spin up-up (triangles), up-down (circles), and down-down (reversed triangles), and total E_{MCA} (squares).

To illustrate the effect of hybridization at the interface of TMs and Fe atoms on MCA, the dependence of E_{MCA} on band filling in the free-standing Os MLs and Os/Fe(001) is presented in Fig. 2(a). The E_{MCA} curves as a function of band filling are hump-shaped for both the free-standing Os ML and the Os/Fe(001). The curve shifts upward by 0.2 eV in the presence of the Fe(001) substrate. The real E_F of Os is denoted by the solid vertical line, and those of Ir and Pt, which have one and two more electrons than Os, are denoted by the dotted and dashed lines in Fig. 2(a), within a rigid band picture. The real E_F of the free-standing Os ML is near the peak, whereas those of the free-standing Ir and Pt MLs are positioned near the minimum. As shown in Table I, the calculated E_{MCA} of the free-standing 5*d* MLs decrease from Os to Pt, which reflects the effect of band filling or the thin solid curve in Fig. 2(a). On the Fe(001) substrate, $E_{MCA}$of the Os ML is substantially reduced, whereas E_{MCA} of the Ir and Pt MLs change in sign from negative to positive. Thus, the Λ-shaped trend shown in Fig. 1(c) is developed in 5*d* TM/Fe(001), which is consistent

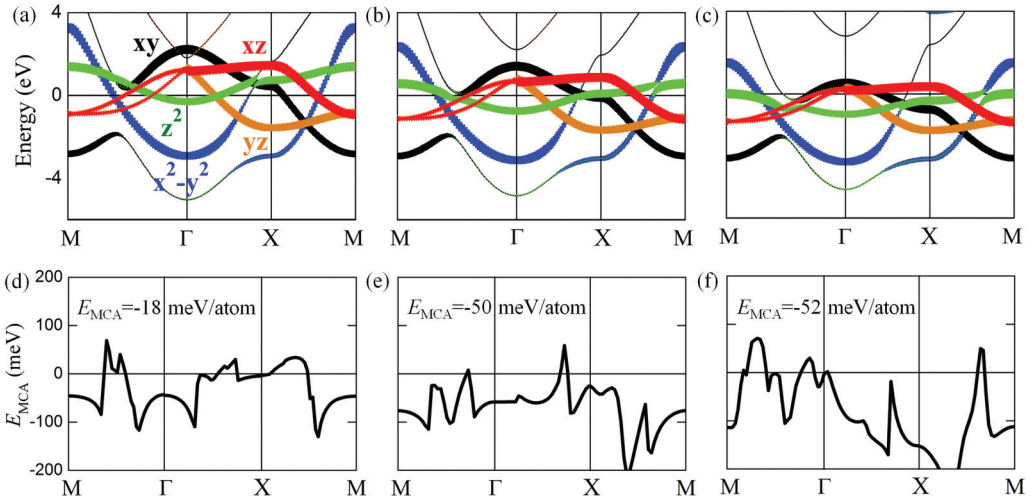

FIG. 3. (Color online) Band structures of the minority spin state along the high symmetry lines in 2D BZ for free-standing (a) Os, (b) Ir, and (c) Pt MLs. The symbol size represents the weight of the d orbitals. The Fermi level is set to zero energy. (d)–(f) The corresponding $E_{\mathrm{MCA}}(\downarrow\downarrow)$ distributions along the high symmetry lines in 2D BZ.

with band filling [see Fig. 2(a)] associated with hybridization at the interface.

Within perturbation theory, E_{MCA} at an atom site is expressed as[34]

$$E_{\mathrm{MCA}}^{\sigma\sigma'} \approx \xi^2 \sum_{o,u} \frac{|\langle o^\sigma|\ell_z|u^{\sigma'}\rangle|^2 - |\langle o^\sigma|\ell_x|u^{\sigma'}\rangle|^2}{\varepsilon_{u\sigma'} - \varepsilon_{o\sigma}}, \qquad (1)$$

where ξ is the SOC coupling constant, and o^σ ($u^{\sigma'}$) and $\varepsilon_{o\sigma}$ ($\varepsilon_{u\sigma'}$) represent eigenstates and eigenvalues of occupied (unoccupied) states in spin state $\sigma(\sigma')$. The total E_{MCA} is the sum of Eq. (1) over all atoms in the unit cell. The decomposition of E_{MCA} into different spin channels, up-up ($\uparrow\uparrow$), up-down ($\uparrow\downarrow$), and down-down ($\downarrow\downarrow$), is straightforward. In Eq. (1), positive and negative contributions are determined by ℓ_z and ℓ_x operators, respectively.

The differences between the values of E_{MCA} with and without the Fe substrate, $\Delta E_{\mathrm{MCA}} = E_{\mathrm{MCA}}(\mathrm{TM/Fe}) - E_{\mathrm{MCA}}$ (free-standing TM ML), are shown in Fig. 2(b). The solid squares represent the total difference, and open symbols represent the decomposed spin-channel contributions. For all cases, $\Delta E_{\mathrm{MCA}}(\downarrow\downarrow) > 0$, whereas $\Delta E_{\mathrm{MCA}}(\uparrow\uparrow) < 0$ and $\Delta E_{\mathrm{MCA}}(\uparrow\downarrow) < 0$. The positive E_{MCA} calculated for 5d TM/Fe(001) must come from $\Delta E_{\mathrm{MCA}}(\downarrow\downarrow) > 0$, i.e., the magnitude of the large negative $E_{\mathrm{MCA}}(\downarrow\downarrow)$ of the free-standing MLs gets much reduced on Fe(001). In addition, ΔE_{MCA} exhibits a trend similar to $\Delta E_{\mathrm{MCA}}(\downarrow\downarrow)$. These results indicate that the $\downarrow\downarrow$ channel plays a crucial role in determining the sign of E_{MCA}. For the Os ML, the relatively small positive $\Delta E_{\mathrm{MCA}}(\downarrow\downarrow)$ is not sufficient to compensate for the negative $\Delta E_{\mathrm{MCA}}(\uparrow\uparrow)$ and $\Delta E_{\mathrm{MCA}}(\uparrow\downarrow)$. Since $\Delta E_{\mathrm{MCA}} < 0$, the total E_{MCA} of Os/Fe(001) is smaller than that of the free-standing Os ML, as mentioned earlier. The discussion regarding the origin of the PMCA of 5d TM/Fe(001) will focus on the $\downarrow\downarrow$ channel contribution.

Prior to determining the electronic origins of the PMCA of 5d TM/Fe(001), the free-standing Os, Ir, and Pt MLs were first analyzed. Their minority spin state bands with orbital projections in 2D BZ are plotted in Figs. 3(a)–3(c). As the atomic number increases from Os to Pt, two features become notable: (i) the d_{z^2} band across E_{F} shifts downward below E_{F} while the other occupied states are steady; (ii) the unoccupied states become narrower and move closer to E_{F}. In addition, the values of $E_{\mathrm{MCA}}(\downarrow\downarrow)$ along the high symmetry lines in the 2D BZ are shown in Figs. 3(d)–3(f). In the free-standing Os ML, the negative $E_{\mathrm{MCA}}(\downarrow\downarrow)$ is dominated by the contribution from $\langle z^2|\ell_x|xz, yz\rangle$ around the Γ and M points. The positive contribution from $\langle x^2 - y^2|\ell_z|xy\rangle$ is small because of the large energy denominator between these two states in Eq. (1). $E_{\mathrm{MCA}} \approx 0$ around the X point because the contributions from $\langle z^2|\ell_x|xz, yz\rangle$ and $\langle x^2 - y^2|\ell_z|xy\rangle$ have similar magnitudes. In the case of Ir, the d_{z^2} band around the Γ and M points shifts down to become further occupied, and the unoccupied d_{xz} band around the Γ point moves closer to E_{F}. The shifts further enhance the negative $E_{\mathrm{MCA}}(\downarrow\downarrow)$ value, which results in the negative E_{MCA} of the free-standing Ir ML. A similar argument can be applied to the free-standing Pt ML. The negative value of $E_{\mathrm{MCA}}(\downarrow\downarrow)$ at the X point become much stronger because the d_{z^2} band is fully occupied and located just below E_{F}, which couples with the unoccupied d_{xz} band just above E_{F}. Moreover, the just unoccupied d_{xy} state around the Γ point results in negligible E_{MCA} around the Γ point.

In Figs. 4(a)–4(c), the d-projected DOSs of the minority spin states of the TMs and the interface Fe in TM/Fe(001) are shown. For comparison, those of the free-standing TM MLs and the clean Fe(001) surface are also presented. It is clear that the presence of Fe(001) strongly affects both the TM and the interface Fe d states: The high DOS peaks of the free-standing ML and the clean Fe(001) surface around E_{F} are spilt into occupied bonding and unoccupied antibonding states due to the significant hybridization between the TM and the interface Fe in TM/Fe(001). The overlap of the peaks of the d states of the TM with those of the interface Fe over a wide energy range indicates strong hybridization.

Projected DOSs for the d_{z^2} and $d_{xz/yz}$ states are presented in Figs. 4(d)–4(f). As discussed in the analysis of the SOC matrices, these two states play a crucial role in determining E_{MCA}. While the $d_{x^2-y^2}$ and d_{xy} states of the in-plane character

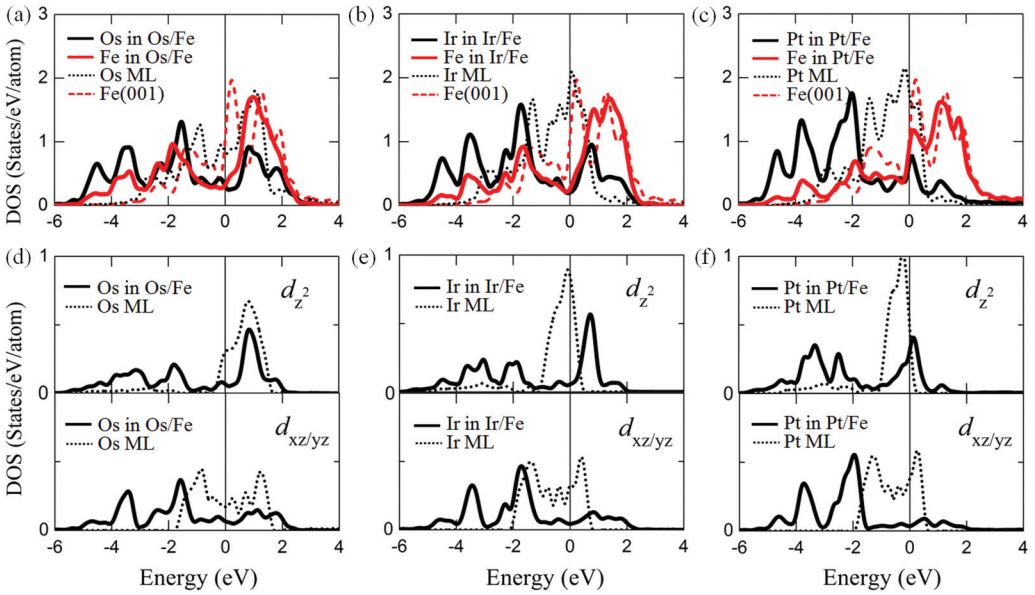

FIG. 4. (Color online) Minority spin d-DOS of the TM (black/dark solid line) and the interface Fe (red/light solid line) of (a) Os/, (b) Ir/, and (c) Pt/Fe(001). Those of the free-standing 5d MLs and the Fe layer at the clean Fe(001) surface are denoted in black/dark dotted and red/light dashed lines, respectively. The d_{z^2}- and $d_{xz/yz}$-projected minority spin DOS of (d) Os, (e) Ir, and (f) Pt MLs with (solid line) and without (dotted line) Fe(001) substrate. The Fermi level is set to zero energy.

are rather rigid, the d_{z^2} and $d_{xz/yz}$ states of the out-of-plane character are significantly influenced by the presence of the Fe(001) substrate via hybridization. The partially occupied d_{z^2} states in the free-standing TM ML are spilt into a sharp unoccupied peak and broad occupied bands. Particularly, the sharp occupied d_{z^2} peaks of the free-standing Ir and Pt MLs, which are responsible for the large negative value of $E_{\mathrm{MCA}}(\downarrow\downarrow)$, shift upward and are located just above E_{F} in the Ir/Fe(001) and Pt/Fe(001). Meanwhile, the $d_{xz/yz}$ bands across E_{F} for the free-standing 5d TM MLs move far below E_{F} for 5d TM/Fe(001) due to strong hybridization with Fe 3d. This upward motion of the d_{z^2} bands and downward motion of the $d_{xz/yz}$ bands increase the energy denominator in the matrix $\langle z^2|\ell_x|xz,yz\rangle$; thus, the presence of the Fe(001) substrate reduces the negative contribution of $E_{\mathrm{MCA}}(\downarrow\downarrow)$ in the 5d MLs. The positive total E_{MCA} values of TM/Fe(001) are due to the reduced negative contribution of $E_{\mathrm{MCA}}(\downarrow\downarrow)$, which arise from the strong hybridization between the Fe-3d and TM-5d bands.

IV. CONCLUSION

In summary, we studied the MCA of a Fe(001) surface capped with 4d (Ru, Rh, and Pd) and 5d (Os, Ir, and Pt) TM MLs using first principles calculations. We predict that the large SOC of 4d and 5d orbitals that are strongly hybridized with the Fe 3d orbitals, except for Pd/Fe(001), would lead to an enhanced PMCA in the TM/Fe(001). In particular, extremely large values of E_{MCA}, as large as $+10$ meV/Ir in Ir/Fe(001), are found for 5d TM/Fe(001). The origin of the large PMCA of 5d TM/Fe(001) is the strong 5d–3d hybridization in the minority spin states, which is identified through detailed analysis of the spin-channel decomposed MCA and electronic structures in the 5d TM MLs with and without the Fe(001) substrate. This system can act as a prototype of the in-depth study of the microscopic origins of the PMCA. It also provides evidence for the role of the magnetic-induced 4d and 5d TMs on MCA, indicating that the TM/Fe interface plays an important role in determining the PMCA of 4d/5d TM/Fe(001).

ACKNOWLEDGMENTS

The research was supported by grants from the Basic Research (2010–0008842) and Priority Research Centers Program (2009–0093818) through the NRF funded by the MOE. S.H.R. acknowledges support from the US DOE (DE-FG02-05ER45372) and supercomputing grant from NERSC. N.P. was supported by the Basic Research Program through NRF funded by MOE(2013R1A1A2007910).

*Present address: Interdisciplinary School of Green Energy and Department of Physics, UNIST, Ulsan 689–798, Korea.
†sonny@u.northwestern.edu
‡schong@ulsan.ac.kr

[1] J. C. Slonczewski, J. Magn. Magn. Mater. **159**, L1 (1996).
[2] A. D. Kent, Nat. Mater. **9**, 699 (2010).
[3] S. Ikeda, K. Miura, H. Yamamoto, K. Mizunuma, H. D. Gan, M. Endo, S. Kanai, J. Hayakawa, F. Matsukura, and H. Ohno, Nat. Mater. **9**, 721 (2010).
[4] J. H. Jung, S. H. Lim, and S. R. Lee, Appl. Phys. Lett. **96**, 042503 (2010).

[5]W.-G. Wang, M. Li, S. Hageman, and C. L. Chien, Nat. Mater. **11**, 64 (2012).
[6]K. Nakamura, T. Akiyama, T. Ito, M. Weinert, and A. J. Freeman, Phys. Rev. B **81**, 220409(R) (2010).
[7]H. X. Yang, M. Chshiev, B. Dieny, J. H. Lee, A. Manchon, and K. H. Shin, Phys. Rev. B **84**, 054401 (2011).
[8]D. C. Worledge, G. Hu, D. W. Abraham, J. Z. Sun, P. L. Trouilloud, J. Nowak, S. Brown, M. C. Gaidis, E. J. O'Sullivan, and R. P. Robertazzi, Appl. Phys. Lett. **98**, 022501 (2011).
[9]T. I. Cheng, C. W. Cheng, and G. Chern, J. Appl. Phys. **112**, 033910 (2012).
[10]Z. Celinski, B. Heinrich, J. F. Cochran, W. B. Muir, A. S. Arrott, and J. Kirschner, Phys. Rev. Lett. **65**, 1156 (1990).
[11]T. Kachel, W. Gudat, C. Carbone, E. Vescovo, S. Blügel, U. Alkemper, and W. Eberhardt, Phys. Rev. B **46**, 12888 (1992).
[12]K. Totland, P. Fuchs, J. C. Grobli, and M. Landolt, Phys. Rev. Lett. **70**, 2487 (1993).
[13]T. Lin, M. A. Tomaz, M. M. Schwickert, and G. R. Harp, Phys. Rev. B **58**, 862 (1998).
[14]R. Bertacco and F. Ciccacci, Phys. Rev. B **57**, 96 (1998).
[15]G. W. R. Leibbrandt, R. van Wijk, and F. H. P. M. Habraken, Phys. Rev. B **47**, 6630 (1993).
[16]L. P. Zhong and A. J. Freeman, J. Appl. Phys. **81**, 3890 (1997).
[17]R. G. Abal, A. M. Llois, and M. Weissmann, J. Phys.: Condens. Matter **8**, 6607 (1996).
[18]J. Dorantes-Davila and G. M. Pastor, Phys. Rev. Lett. **81**, 208 (1998).
[19]Y. Mokrousov, G. Bihlmayer, S. Heinze, and S. Blügel, Phys. Rev. Lett. **96**, 147201 (2006).
[20]V. L. Moruzzi and P. M. Marcus, Phys. Rev. B **39**, 471 (1989).
[21]H. Chen, N. E. Brener, and J. Callaway, Phys. Rev. B **40**, 1443 (1989).
[22]O. Eriksson, R. C. Albers, and A. M. Boring, Phys. Rev. Lett. **66**, 1350 (1991).
[23]P. Gambardella, S. Rusponi, M. Veronese, S. S. Dhesi, C. Grazioli, A. Dallmeyer, I. Cabria, R. Zeller, P. H. Dederichs, K. Kern, C. Carbone, and H. Brune, Science **300**, 1130 (2003).
[24]T. O. Strandberg, C. M. Canali, and A. H. MacDonald, Nat. Mater. **6**, 648 (2007).
[25]R. J. Xiao, D. Fritsch, M. D. Kuz'min, K. Koepernik, H. Eschrig, M. Richter, K. Vietze, and G. Seifert, Phys. Rev. Lett. **103**, 187201 (2009).
[26]B. Újfalussy, L. Szunyogh, P. Bruno, and P. Weinberger, Phys. Rev. Lett. **77**, 1805 (1996).
[27]M. Tsujikawa and T. Oda, Phys. Rev. Lett. **102**, 247203 (2009).
[28]E. Wimmer, H. Krakauer, M. Weinert, and A. J. Freeman, Phys. Rev. B **24**, 864 (1981).
[29]J. P. Perdew, K. Burke, and M. Ernzerhof, Phys. Rev. Lett. **77**, 3865 (1996).
[30]L. Hedin and B. I. Lundqvist, J. Phys. C: Solid State Phys. **4**, 2064 (1971).
[31]X. Wang, R. Q. Wu, D. S. Wang, and A. J. Freeman, Phys. Rev. B **54**, 61 (1996).
[32]R. Q. Wu and A. J. Freeman, J. Magn. Magn. Mater. **200**, 498 (1999).
[33]S. C. Hong, J. I. Lee, and A. J. Freeman, J. Magn. Magn. Mater. **99**, L45 (1991).
[34]D. S. Wang, R. Q. Wu, and A. J. Freeman, Phys. Rev. B **47**, 14932 (1993).